On the bifurcation curve for an elliptic system of FitzHugh-Nagumo type

Guido Sweers
Applied Mathematical Analysis
Delft University of Technology
PObox 5031, 2600 GA Delft
Netherlands

William C. Troy
Mathematics Department
University of Pittsburgh
Pittsburgh,Pa. 15260
U.S.A.

Abstract

We study a system of partial differential equations derived from the FitzHugh-Nagumo model. In one dimension solutions are required to satisfy zero Dirichlet boundary conditions on the interval $\Omega = (-1, 1)$. Estimates are given to describe bounds on the range of parameters over which solutions exist; numerical computations provide the global bifurcation diagram for families of symmetric and asymmetric solutions. In the two dimensional case we use numerical methods for zero Dirichlet boundary conditions on the square domain $\Omega = (-1, 1) \times (-1, 1)$. Numerical computations are given both for symmetric and asymmetric, and for stable and unstable solutions.

1 Introduction

The FitzHugh-Nagumo type model problem that we study originates in the following system of two coupled parabolic second order differential equations:

$$u_t = \varepsilon^2 \Delta u + f(u) - \delta v \quad \text{and} \quad v_t = \Delta v + u - \gamma v \quad \text{in } \Omega \times \mathbb{R}^+ \subset \mathbb{R}^{n+1}. \tag{1}$$

The parameters $\varepsilon > 0$, $\gamma \geq 0$ and δ are real and

$$f(u) = u(1-u)(u-a) \text{ with } a \in \left(0, \tfrac{1}{2}\right).$$

We are interested in stationary solutions of system (1) on bounded domains with Dirichlet boundary conditions, that is, in pairs of functions (u, v) that satisfy the associated nonlinear elliptic system:

$$\begin{cases} -\varepsilon^2 \Delta u = f(u) - \delta v & \text{in } \Omega, \\ -\Delta v = u - \gamma v & \text{in } \Omega, \\ u = v = 0 & \text{on } \partial\Omega, \end{cases} \tag{2}$$

where Ω is a bounded domain in $\mathbb{R}^n$. Specifically, fixing ε a small number, we would like to understand the dependence on the parameter δ.

AMS subject classifications: 34B15, 34C23, 93C15, 34C11.

1.1 Physical background

The original one-dimensional parabolic differential equations (1), named after FitzHugh and Nagumo [11, 20], were derived to serve as a prototype simplification of the original Hodgkin-Huxley nerve conduction equations [14]. Both the parabolic as well as the corresponding elliptic system have attracted much interest since the model is relatively simple yet retains the physically important characteristics of excitability and bistability. For example, the FitzHugh-Nagumo has served as the basis for a model of cardiac excitation [25, 1]. We also mention the recent work of Goldstein et al [16], in which a modification of (1) is proposed as a model for the development of labyrinth pattern formation in an activator-inhibitor system. In this study u plays the role of activator, v is the inhibitor, ε multiplies only the term v_t in (1), and an additional function is added to the u equation to control the phenomenon of symmetry breaking. When $\varepsilon = 0$ (i.e. the fast inhibitor limit) it is shown that spots or stripes can be destabilized into space–filling structures called labyrinths. For larger ε (i.e. slow inhibition) it is shown in [15] that the labyrinth destabilizes into spiral waves. In other physical settings it is necessary for ε to multiply the diffusion term in the first equation [19, 22]. Here a slow diffusion phenomenon occurs when ε is small. For example, in [16] chemical pattern formation and relaxation is modeled by this type of system in both one and two dimensions. Thus, the FitzHugh-Nagumo system has come to play a fundamental role in understanding pattern formation in higher order excitable, bistable systems (see also [10], [17] and [18]).

1.2 Mathematical objective

In this paper we investigate properties of solutions of (2) over a range of parameters complementary to those considered in the activator-inhibitor studies described above. Our main interest is to provide a detailed understanding of the different types of solutions when ε is small and fixed and δ is allowed to vary. Using analytical and numerical techniques, we will determine how the global structure of solutions depends on the parameter δ when $\varepsilon > 0$ is small. Our investigation includes both the one and two dimensional cases. To make the analysis more tractable we find it convenient to fix $\gamma = 0$.

Our study is also motivated by a recent paper ([24]) in which analytical methods were used to show that for $\delta \in [0, \delta_1)$ a boundary layer solution exists for $\Omega \subset \mathbb{R}^n$ which is a local minimizer of an appropriate energy functional. Moreover, it was shown that there exists a $\delta_0 \in (0, \delta_1)$ such that the global minimizer has lower energy than the boundary layer solution. Numerical evidence was given that this solution has both an internal and a boundary layer. With the trivial solution this gives three local minimizers in that δ-range. Generically, multiple mountain pass solutions will exist in between. The main question that is addressed in this paper is how these solutions are connected (in both one and two dimensions) and of which type they will be. Due to the complexity of the system, that is, the singularity appearing for $\varepsilon \downarrow 0$, and the noncooperative structure of (2), which prevents order preserving methods based on the maximum principle, analytical techniques will not suffice, especially in the two-dimensional case. Thus, numerical means seem to form the only remaining approach. The numeric part is described below and will be restricted to Ω being an interval in one dimension and a square in two dimensions.

1.3 Numerics

First, a powerful numerical ode-tool (Auto97 [7]) is used to describe the global bifurcation diagram for $\delta \mapsto u(\delta)$ in one space dimension. It allows us to address several ranges for

ε. Next, using the insight gained in our investigation of the one–dimensional problem as a guide, we pursue our study of the two–dimensional case. Here we will fix ε to be small. We begin by using a rather standard numerical iteration scheme that finds solutions which are local minimizers (i.e. 'stable' solutions) of an energy function in 2 dimensions. Finally, we will adapt a saddle-point algorithm of Choi and McKenna ([2]) to find unstable solutions (i.e. solutions which are not local minimizers), also in 2 dimensions. This last part is the trickiest and requires the development of a new algorithm to handle delicate numerical issues. The main difficulty that one encounters here is that all but one of these solutions are of the form 'trivial solution plus peak', which means that a numerical approximation almost ignores the location of the peak: any interior peak approximately solves the boundary condition. To overcome this problem a sub-algorithm is introduced, which we call 'tango', that compares the approximating peak with the similar peaks shifted one grid-size in the north, respectively east, south and west directions. The numerical outcome on a square is that we obtain a new solution which is *asymmetric*, and the preferred position of its peak is near a corner (see Figures 17 and 20, right panels). This coincides with the result of Dancer and Wei in [5] for the scalar equation $-\varepsilon^2\Delta u = f(u) - c$ with c a small constant: they showed that the peaks are located near, roughly described, the most convex boundary points. Other peak shaped solutions are obtained by using a symmetry-ansatz (see Figure 20 - left panel, and Figure 21). Only one mountain pass solution has a different shape as a peak upwards from 0, being the pass between the boundary layer in the double layer solution; it has a boundary layer with a downward peak in the interior (see Figures 18 and 19, right panels). Not only is this solution obtained by the newly designed algorithms, but the numerical outcome shows a clear difference between this downward peak (a mountain pass) and the solution with both boundary and internal layer (a minimizer). This stands in clear contrast to the predictions for (2) given in [6] where existence of a minimizer with double layer is disputed. There is no real contradiction since Dancer and Yan study in [6] the limit case $\varepsilon \to 0$. We come back to this in section 5.

2 Overview

Since the crucial parameter for problem (2) is δ, we will set $\gamma = 0$ and $a = \frac{1}{4}$ and consider small fixed values of ε. For small fixed $\varepsilon > 0$ we are primarily interested in the dependence of solutions on δ for $\delta > 0$. However, as will become clear in forthcoming sections, it is also important to consider negative values of δ in order to obtain a global understanding of the structure of entire families of solutions. We note that for $\delta \leq 0$ the system (2) is cooperative. Cooperative elliptic systems share many properties with single elliptic equations and hence are more easily handled analytically.

As was mentioned earlier, the present paper is motivated by the results in [24] for the corresponding partial differential equations system (1). There, the scaling by δ appeared in the second equation but presently the equivalent system (2) will be more convenient. In [24] evidence for the two-dimensional problem was given to show that two 'stable' solutions coexist for a certain range of $\delta > 0$, one of which exhibits a boundary layer behavior (see Figure 17, left panel), and a second one where, next to this boundary layer, an internal jump appears in the graph of u (see Figure 18, left panel). Although it was guessed that these two solutions (δ_1, u_1) and (δ_1, u_2) were on the same bifurcation curve, no evidence for this conjecture was given. Note that since the v-component is uniquely determined by u there is no ambiguity to just consider pairs (δ, u).

Another question raised in [24] was how such a curve would continue as δ varies, with

$\varepsilon > 0$ held fixed. By analytical arguments ([23]) it is known that such a curve cannot just stop. It seems that the only way for the curve to leave the set $\{(\delta, u)\,; \delta > 0 \text{ and } \|u\|_\infty < M\}$ for appropriate M is at $\delta = 0$. However, for $\delta = 0$ we just have one differential equation which is known to have exactly 2 nontrivial solutions for small, positive ε ([26]). Note that the trivial function $(u, v) \equiv (0, 0)$ is also a solution for all δ. In [24] it was shown that the solution at the furthest known point in the (δ, u) bifurcation diagram is completely different from the second solution at $\delta = 0$, hence the connection was most mysterious. To help unravel this mystery, and to understand the mechanisms responsible for pattern formation in problem (2) our investigation will address the following questions and issues:

(i) For the one–dimensional problem, what is the global bifurcation diagram of solutions for small values of $\varepsilon > 0$? Here the goal is to obtain a precise description of the types of solutions (e.g. symmetric or asymmetric), their shapes and their multiplicity in terms of δ. Both for computational reasons and because the bifurcation diagram tends to become more and more complicated ε cannot be chosen too small.

(ii) For the more complicated two–dimensional problem use the results of (i) to help determine the global behavior of families of solutions as δ varies, again for appropriately selected small values ε. As in the one dimensional case the goal is to determine properties of both symmetric and asymmetric solutions, including existence and multiplicity, and also the shapes of solutions. New algorithms are developed to determine these properties as well as the stability of solutions (i.e. whether they are local or global minimizers). It is hoped that further refinements of these algorithms will lead to new insights into the properties of the full time-dependent problem (1) when it is viewed as a dynamical system. Here, we expect the local and global mimizers (i.e. the stable solutions) to form essential elements of the attractor for the system. To help characterize the attractor it is important to determine the basins of attraction of the local and global mimizers. We expect that further studies of properties of mountain pass solutions (i.e. the unstable solutions) which seperate minimizers will provide valuable insight into delineating the borders of the basins of attraction.

In Section 3 we give our analytical results for the one-dimensional case. We begin with the development of a Green's function which allows for the integral representation of v in terms of u when (u, v) solves (2). For simplicity we take $\gamma = 0$ and we expect a similar behavior for γ near 0. Section 3.1 presents several important results for the special case $\delta = 0$. When $\delta \neq 0$, we show in Section 3.2 how families of solutions come into existence via a bifurcation from the trivial solution at critical values of δ. Then, in order to obtain the best possible description of these families of solutions, we derive several a-priori estimates in Section 3.3. Finally, to augment our analytical results, Section 4.1 gives a complete numerical analysis of the global behavior of families of solutions in terms of δ for selected small, positive values of ε. Motivated by results in the one-dimensional case, we then turn in Section 4.2 to give further results on the full two-dimensional problem. Finally, in Section 5 we summarize our results and give suggestions for further study.

3 Analytical results

As was stated in Section 1, we assume that $\gamma = 0$ and $a = \frac{1}{4}$. Thus, all of our analytical and numerical results will be for the following problem:

$$\left\{\begin{array}{rcll} -\varepsilon^2 u'' & = & f(u) - \delta v & \text{for } -1 < x < 1; \\ -v'' & = & u & \text{for } -1 < x < 1; \\ u = v & = & 0 & \text{for } x \in \{-1, 1\}, \end{array}\right. \tag{3}$$

where

$$f(u) = u(1-u)\left(u - \frac{1}{4}\right). \tag{4}$$

We first note that the v component of a solution (u, v) of (3)-(4) satisfies

$$v(x) = (\mathcal{G}u)(x) := \int_{x=-1}^{1} g(x, s)\, u(s)\, ds, \tag{5}$$

with the Green function g defined by

$$g(x, y) = \left\{\begin{array}{ll} \frac{1}{2}(1-x)(1+y) & \text{if } x \geq y, \\ \frac{1}{2}(1-y)(1+x) & \text{if } x < y. \end{array}\right.$$

Thus, a pair $(\delta, u) \in \mathbb{R} \times C[-1, 1]$ will be called a solution problem (3)-(4) if $u \in C^2[-1, 1]$, v is as in (5), and the equations and boundary conditions are satisfied.

We will classify the different types of solutions of (3)-(4) according to their basic properties. These include positive solutions, as well as symmetric and asymmetric solutions. A solution (u, v) of (3)-(4) is called a positive solution if $u(x) > 0$ for all $x \in (-1, 1)$. From (5) it follows that, if u is positive on $(-1, 1)$, then v is also positive on $(-1, 1)$.

Next, we consider solutions of (3)-(4) which satisfy

$$u'(0) = v'(0) = 0. \tag{6}$$

It follows from (3)-(4) that any solution satisfying (6) must also satisfy

$$(u(x), v(x)) = (u(-x), v(-x)) \ \forall x \in (-1, 1).$$

Thus, a solution satisfying (6) is symmetric with respect to $x = 0$, and is therefore classified as a symmetric solution. If a solution of (3)-(4) does not satisfy (6) then it is called an asymmetric solution. In Figure 1 in the next section we illustrate an example of a solution which is both positive and symmetric. In Section 4.1 we shall see that families of solutions exist which are either non-positive or asymmetric (or both).

3.1 The single equation

If we set $\delta = 0$ we find that the system (3) uncouples and reduces to

$$\left\{\begin{array}{rcll} -\varepsilon^2 u'' & = & f(u) & \text{for } -1 < x < 1; \\ -v'' & = & u & \text{for } -1 < x < 1; \\ u = v & = & 0 & \text{for } x \in \{-1, 1\}. \end{array}\right. \tag{7}$$

The boundary value problem satisfied by the u in problem (7) is well studied (see, for example, [26] or [12]), and in the next lemma we summarize the known results.

Lemma 1 *If $\varepsilon \in (0, \varepsilon_0)$ with $\varepsilon_0 > 0$ sufficiently small, then there are exactly two nontrivial solutions of (7). Denoting the u components by u_1, u_2 we find that $1 > u_1(x) > u_2(x) > 0$ for all $-1 < x < 1$. The solution u_1 is of boundary layer type; u_2 is a so-called peak-solution (see Figure 1).*
One even has the following: there are $c_i > 0$ such that for all $\varepsilon \in (0, \varepsilon_0)$ and $x \in (-1, 1)$

$$\begin{array}{ccccc} 1 - e^{\frac{-c_1(1-|x|)}{\varepsilon}} & < & u_1(x) & < & 1, \\ \theta\left(e^{\frac{-c_2|x|}{\varepsilon}} - e^{\frac{-c_2}{\varepsilon}}\right) & < & u_2(x) & < & (\theta + c_3\varepsilon)\left(e^{\frac{-c_4|x|}{\varepsilon}} - e^{\frac{-c_4}{\varepsilon}}\right), \end{array}$$

where $\theta \in (0,1)$ is the unique number such that $\int_0^\theta f(s)\,ds = 0$. As a consequence we have $\lim_{\varepsilon \downarrow 0} v_1(x) = \frac{1}{2} - \frac{1}{2}x^2$ and $\lim_{\varepsilon \downarrow 0} v_2(x) = 0$.

Remark 2 *One may show that there exists a critical value $\varepsilon_1 > 0$ such that for all $\varepsilon > \varepsilon_1$ there are no positive solutions. This number ε_1 satisfies $\varepsilon_1 < \frac{3}{4\pi}$. Indeed, the fact that*

$$\varepsilon^2 u'' + \left(\tfrac{3}{8}\right)^2 u = u\left(u - \tfrac{5}{8}\right)^2 \geq 0 \text{ for } u \geq 0,$$

and even strictly positive if $0 < u \neq \frac{5}{8}$, shows that for positive solutions u the Wronskian of $\cos\left(\frac{3}{8\varepsilon}\cdot\right)$ and $u(\cdot)$,

$$W(x) := \cos\left(\tfrac{3}{8\varepsilon}x\right) u'(x) + \tfrac{3}{8\varepsilon}\sin\left(\tfrac{3}{8\varepsilon}x\right) u(x)$$

is strictly increasing if $\cos\left(\frac{3}{8\varepsilon}x\right) \geq 0$. Since $W(0) = 0$ the assumption $\frac{3}{8\varepsilon} < \frac{\pi}{2}$ yields $W(1) \leq 0$, a contradiction. Hence $\varepsilon < \frac{3}{4\pi} \approx 0.23873$. The sharpness of this upper bound is borne out by our numerical experiments in Section 4.1.

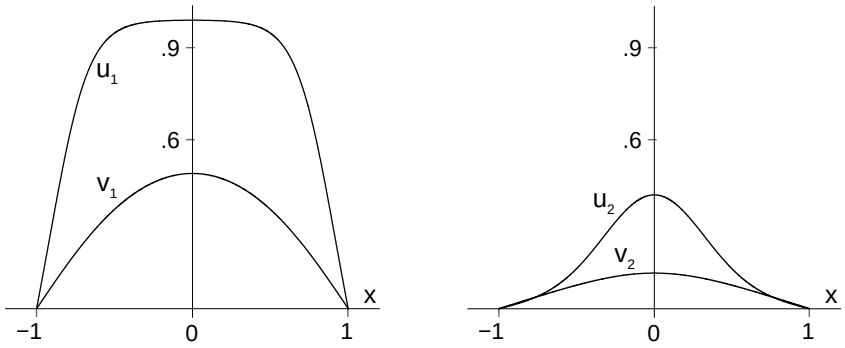

Figure 1: *Solutions u_1, v_1 (left) and u_2, v_2 (right) of (7). The parameters are $\varepsilon = .1$, and $\delta = 0$.*

Proof. Consider the initial value problem $-v'' = f(v)$ with $v'(0) = 0$ and $v(0) = v_0 > 0$. One shows that v has a zero if and only if $\int_v^{v_0} f(s)\,ds > 0$ for all $v \in [0, v_0)$. Indeed, since $v'(t) < 0$ holds at least up to a first zero and

$$v'(t) = -\sqrt{2\int_{v(t)}^{v_0} f(s)\,ds}$$

this claim follows. For the f above this condition reduces to $v_0 \in (\theta, 1)$. Notice that, if $v_0 = \theta$, then $v(t) \downarrow 0$ as $t \to \infty$; for $v_0 = 1$ we have $v(t) \equiv 1$. By considering the so-called time-map ([26])

$$T(v_0) = \frac{1}{\sqrt{2}} \int_0^{v_0} \frac{ds}{\sqrt{F(v_0) - F(s)}},$$

where $F(s) = \int_0^s f(v)\,dv$, one finds that $T'(v_0) > 0$ for $v_0 \in (\theta, \theta+\delta) \cup (1-\delta, 1)$. The appropriate rescaling shows the first claim of the lemma. For the remaining estimates we refer to [12]. ■

Remark 3 *In the radially symmetric n-dimensional case, that is u'' replaced by $u'' + \frac{n-1}{r}u'$, the existence of exactly two solutions has been proven in [13].*

3.2 Bifurcation from the zero solution

Since $f(0) = 0$ the trivial function $(u, v) \equiv 0$ is a solution of (7) for all $\delta \in \mathbb{R}$. A number δ^* is called a bifurcation point for bifurcations from the trivial solution if there is a sequence of solutions $\{(\delta_n, u_n)\}_{n\in\mathbb{N}}$ with $\delta_n \to \delta^*$ and $u_n \to 0$. By $u_n \to 0$ we denote convergence in $C[0,1]$.

Lemma 4 *The bifurcation points of (7) for bifurcations from the trivial solution are $\left\{-\frac{1}{16}\left(\varepsilon^2\pi^2m^2+1\right)\pi^2m^2; m \in \mathbb{Z}^+\right\}$.*

Proof. We set

$$X = \left\{u \in C^2[0,1]; u(-1) = u(1) = 0\right\} \text{ and } Y = C[0,1],$$

and define $\mathcal{B}_\varepsilon : \mathbb{R}\times X \to Y$ by

$$\mathcal{B}_\varepsilon(\delta, u) := -\varepsilon^2 u'' - F(u) + \delta\mathcal{G}u,$$

where $F(u)(x) := f(u(x))$. Any solution $u \in X$ of the functional equation

$$\mathcal{B}_\varepsilon(\delta, u) = 0 \tag{8}$$

is a solution of system (7) and vice versa. We remark that the mapping $\mathcal{B}_\varepsilon$ is C^2 and denoting the Frechet derivative with respect to u by d we find

$$d(\mathcal{B}_\varepsilon(\delta, u))(v) = -\varepsilon^2 v'' - f'(u)v + \delta\mathcal{G}v.$$

A necessary condition for a bifurcation point is that there exists a $\phi \in X\setminus\{0\}$ such that

$$d(\mathcal{B}_\varepsilon(\delta^*, 0))(\phi) = 0.$$

Such ϕ is a nontrivial solution for

$$\begin{cases} \varepsilon^2\phi^{(iv)} - \frac{1}{4}\phi'' = -\delta^*\phi \text{ in } (-1,1), \\ \phi(-1) = \phi(1) = 0, \\ \phi''(-1) = \phi''(1) = 0. \end{cases} \tag{9}$$

The eigenvalues/functions for (9) can be directly computed. A more formal approach simplifies these computations. Using that both (9) and

$$\begin{cases} -\phi'' = \lambda\phi \text{ in } (-1,1), \\ \phi(-1) = \phi(1) = 0, \end{cases} \tag{10}$$

are essentially self-adjoint, the eigenfunctions $\{\phi_m\}_{m=1}^\infty$, with

$$\phi_m(x) := \sin(m(x+1)\pi/2),$$

form a complete orthonormal system in $L_2(-1,1)$. Since every eigenfunction for (10) yields an eigenfunction for (9) and since that system is complete, the eigenfunctions coincide. By direct computation the respective eigenvalues δ and λ correspond by

$$\delta^* = -\tfrac{1}{4}\lambda - \varepsilon^2\lambda^2,$$

Hence from $\lambda_m = \frac{1}{4}\pi^2 m^2$ we find

$$\delta^* \in \left\{\delta_m := -\tfrac{1}{16}\pi^2 m^2\left(1+\varepsilon^2\pi^2 m^2\right); m \in \mathbb{Z}^+\right\}. \tag{11}$$

To show that at each number in (11) indeed a bifurcation does occur we use [4]. For δ_m in (11) the functional $\mathcal{B}_\varepsilon$ satisfies the conditions of [4, Theorem 1.7]:

(a) $\mathcal{B}_\varepsilon(\delta,0) = 0$ for all $\delta \in \mathbb{R}$,

(b) The partial derivatives $\frac{\partial}{\partial\delta}\mathcal{B}_\varepsilon$, $d\mathcal{B}_\varepsilon$ and $\frac{\partial}{\partial\delta}(d\mathcal{B})_\delta$ exist and are continuous,

(c/d) $N(d\mathcal{B}_\varepsilon(\delta_m,0)) = span[\phi_m] = Y/R(d\mathcal{B}_\varepsilon(\delta_m,0))$. Indeed, $\mathcal{G}\phi_m = \lambda_m^{-1}\phi_m$ and

$$d\mathcal{B}_\varepsilon(\delta_m,0)(v) = -\varepsilon^2 v'' - \tfrac{1}{4}v + \delta_m\mathcal{G}v$$

$$= \varepsilon^{-2}\left(-\tfrac{\partial^2}{\partial x^2} + \tfrac{1}{4}\pi^2 m^2\right)\circ\left(1+\tfrac{1}{4}\left(\varepsilon^{-2}+\pi^2 m^2\right)\mathcal{G}\right)v.$$

Then, for Z a complement of $span[\phi_m]$ in Y, there exists an open interval $I \ni 0$ and continuously differentiable functions $\delta_m(\cdot): I \to \mathbb{R}$ and $\psi_m(\cdot): I \to Z$, with $\delta_m(0) = \delta_m$ and $\psi(0) = 0$, such that

$$\mathcal{B}_\varepsilon(\delta_m(s), s\phi_m + s\psi_m(s)) = 0.$$

This curve of solutions is unique in the sense that if (δ,u) near $(\delta_m,0)$ satisfies $\mathcal{B}_\varepsilon(\delta,u)=0$, then either $u=0$ or $(\delta,u) = (\delta_m(s), s\phi_m + s\psi_m(s))$ for some $s \in I$. ■

3.3 A priori bounds

Using the differential equations and the observation that, for $a \in \left(0,\frac{1}{2}\right)$,

$$(1+a)u^3 \le 1 + au^2 + \frac{5}{8}u^4,$$

one finds

$$\begin{aligned} 0 &\le \int_{-1}^{1}\left(\varepsilon^2\left(u'\right)^2 + \delta\left(v'\right)^2\right)dx = \int_{-1}^{1} uf(u)\,dx = \\ &= \int_{-1}^{1}\left(-u^4 + (a+1)u^3 - au^2\right)dx \le \\ &\le \int_{-1}^{1}\left(1-\tfrac{3}{8}u^4\right)dx \le 2 - \tfrac{3}{8}\int_{-1}^{1}u^4 dx. \end{aligned} \tag{12}$$

Hence, we find

$$\int_{-1}^{1} u^4 dx \le \frac{16}{3}, \tag{13}$$

$$\int_{-1}^{1}\left(u'\right)^2 dx \le 2\varepsilon^{-2}, \tag{14}$$

$$\int_{-1}^{1}\left(v'\right)^2 dx \le 2\delta^{-1}. \tag{15}$$

By (13) and the second equation of (2) we find that $\|v''\|_{L^4} \leq \sqrt[4]{\frac{16}{3}}$. Since the Green function is bounded it follows that

$$|v(x)| \leq \left| \int_{-1}^{1} g(x,s)\, v''(s)\, ds \right| \leq \tfrac{1}{2} \int_{-1}^{1} \left| v''(s) \right| ds \leq 2^{-\frac{1}{4}} \left\| v'' \right\|_{L^4} \leq 1.3.$$

By this uniform bound for v one finds

$$\begin{aligned} f(u) - \delta v &\leq f(u) + 1.3\,\delta \leq (1-u)^3 + 1.3\,\delta \quad \text{for } u > 1, && (16) \\ f(u) - \delta v &\geq f(u) - 1.3\,\delta \geq -u^3 - 1.3\,\delta \quad \text{for } u < 0. && (17) \end{aligned}$$

Since at an interior maximum $\bar{x}$ it holds that $-u''(\bar{x}) > 0$, (16) implies $u < 1 + \sqrt[3]{1.3\,\delta}$. A similar argument for an interior minimum $\underline{x}$, where $-u''(\underline{x}) < 0$, yields $u > -\sqrt[3]{1.3\,\delta}$. Combining with (14)

$$|u(x)| \leq \left| \int_{-1}^{x} u'(s)\, ds \right| \leq \sqrt{2} \left(\int_{-1}^{1} u'(s)^2\, ds \right)^{1/2} \leq 2\varepsilon^{-1},$$

we obtain:

Lemma 5 *For any solution (δ, u) of (2) with $\delta \geq 0$ and $\varepsilon > 0$*

$$\begin{aligned} -1.1\ \delta^{\frac{1}{3}} &\leq u(x) \leq 1 + 1.1\,\delta^{\frac{1}{3}}, && (18) \\ -2\varepsilon^{-1} &\leq u(x) \leq 2\,\varepsilon^{-1}. && (19) \end{aligned}$$

4 Numerical Results

4.1 In one dimension

In this section we use the continuation program Auto97 ([7]) to determine the global behavior of families of solutions of our boundary value problem which, for convenience, is restated below:

$$\begin{cases} -\varepsilon^2 u'' = f(u) - \delta v & \text{for } -1 < x < 1; \\ -v'' = u & \text{for } -1 < x < 1; \\ u = v = 0 & \text{for } x \in \{-1, 1\}, \end{cases} \tag{20}$$

where $\varepsilon > 0$ and δ are real parameters, and

$$f(u) = u(1-u)\left(u - \tfrac{1}{4}\right).$$

The numerical procedure we use is the following: first, we select specific values for $\varepsilon > 0$ and δ, and solve (20) using the ordinary differential equation program XPPAUT ([8]). Next, keeping ε fixed, we use Auto97 to continue the solution as δ varies.

We have found that families of solutions of (20) come into existence via a bifurcation from the trivial solution $(u(x), v(x)) \equiv (0,0)$ at critical values of δ when ε is fixed. In Lemma 4 we developed a formula for the bifurcation values of δ. The formula in Lemma 4 involves an integer m. As we shall see, the value $m = 1$ plays an important role in our study of (20). Thus, for easy reference we restate the formula when $m = 1$:

$$\delta_1(\varepsilon) = -\frac{1}{16}(\varepsilon^2\pi^2 + 1)\pi^2 \tag{21}$$

4.1.1 $\varepsilon > .2387$

To begin our investigation we recall from Remark 2 in Section 3.1 that there is a critical value ε_1 in the interval $(0, .2387)$ such that if $\delta = 0$ and $\varepsilon > \varepsilon_1$ in (20) then no positive solution exists. When $\varepsilon > \varepsilon_1$ it is natural to ask if such solutions can exist for $\delta \neq 0$. Thus, setting $\varepsilon = .25$, we pursue this question and find that positive solutions do exist, but only for a negative range of δ values. The bifurcation diagram in Figure 2 shows that a family of solutions of (20) exists for $-\infty < \delta < \delta_* \approx -.0746$.

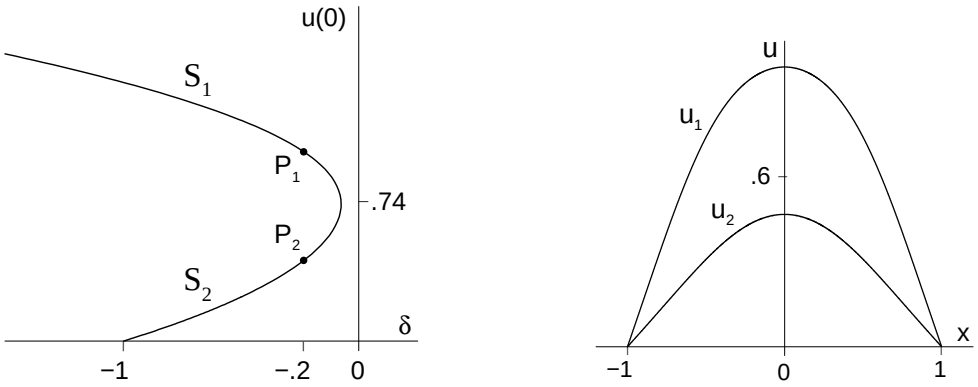

Figure 2: *Bifurcation curve of positive, symmetric solutions for* $\varepsilon = .25$ *and corresponding solutions* u_1 *and* u_2 *at* P_1 *and* P_2 *respectively.*

Each point on the diagram corresponds to a positive, symmetric solution of (20). The vertical axis gives $u(0)$, the value of the solution at $x = 0$. Figure 2 shows the bifurcation curve. The upper part, the stable solutions, is labeled by S_1, and S_2 denotes the lower part or saddle points. At $\delta_* \approx -.0746$ the two parts meet at the 'knee' in the diagram. S_1 appears to exist for all $\delta < \delta_*$, and increases in magnitude as δ decreases. S_2 comes into existence via a bifurcation from the trivial solution $(u, v) = (0, 0)$ at $\delta_1 \approx -.99735$. This value is in excellent agreement with the value predicted when $\varepsilon = .25$ in formula (21) given above. Thus, there is an interval of δ values in which *two* solutions coexist. Setting $\delta = -.2$, we illustrate the u components of these solutions in Figure 2. The v components of these solutions are qualitatively the same as the v components of the solutions shown in Figure 1 in Section 3.1. Also, we note that on the interval $[-1, 1]$, the maximum value of the u component of each solution in Figure 2 occurs at $x = 0$. We have found that this property holds along the entire diagram in Figure 2.

4.1.2 ε **in** $[.2, .2387)$

We lower ε from .25 and find that $\varepsilon_1 \approx .223818$ is the first critical value described above. That is, when $\varepsilon = \varepsilon_1$ our computations in Figure 3 show that positive solutions exist if and only if $\delta \leq 0$. Again, we find that all points along the bifurcation curve correspond to positive, symmetric solutions of (20), and that $u(0)$ represents the maximum value of the solution on $[-1, 1]$.

Lowering ε further, we find that the bifurcation curve enters the region $\delta > 0$ in the $(\delta, u(0))$ plane. This is illustrated by the right hand side picture in Figure 3 for the value $\varepsilon = .2$ As in the cases considered above, we find that all solutions along the bifurcation curve are positive and symmetric, and that $u(0)$ represents the maximum value of the solution on $[-1, 1]$.

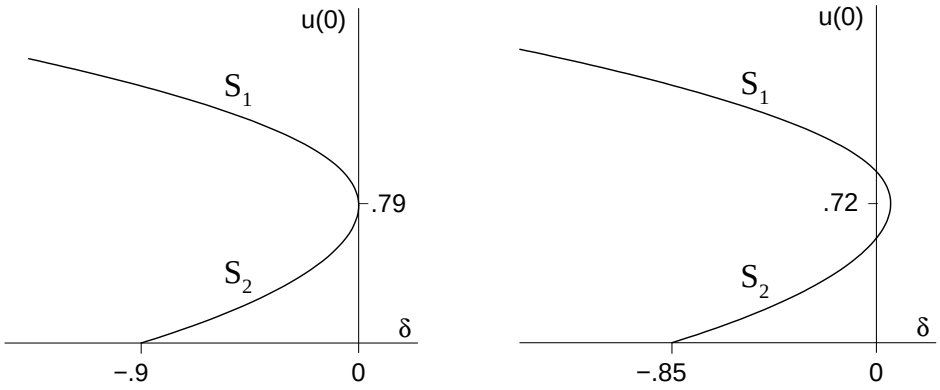

Figure 3: *Bifurcation curve of positive, symmetric solutions at* $\varepsilon = .22381$*, respectively* $\varepsilon = .2$*.*

4.1.3 ε in $[.1, .2)$

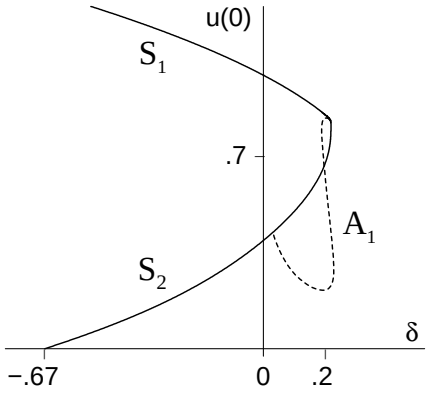

Figure 4: *Bifurcation curves of symmetric and asymmetric solutions:* $\varepsilon = .1$

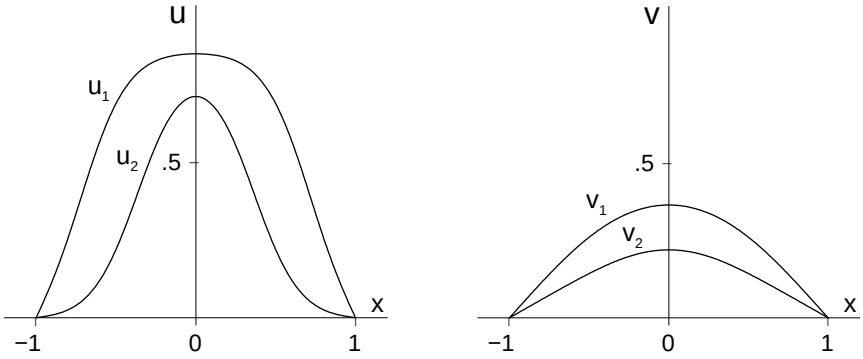

Figure 5: *Symmetric solutions* u_1, u_2 *(left) and* v_1, v_2 *(right) of (20). The parameters are* $\varepsilon = .1$*, and* $\delta = .2$

We continue to lower ε and find a second critical value, $\varepsilon_2 \approx .134$, at which a branch of asymmetric solutions comes into existence by a bifurcation from the branch of symmetric solutions. In Figure 4 we set $\varepsilon = .1$ and compute the lower and upper branches of symmetric solutions (denoted by the solid curves S_1 and S_2), and also the branch A_1 (denoted by the dashed curve) of asymmetric solutions. In Figure 5 we set $\varepsilon = .1$ and $\delta = .2$ and show

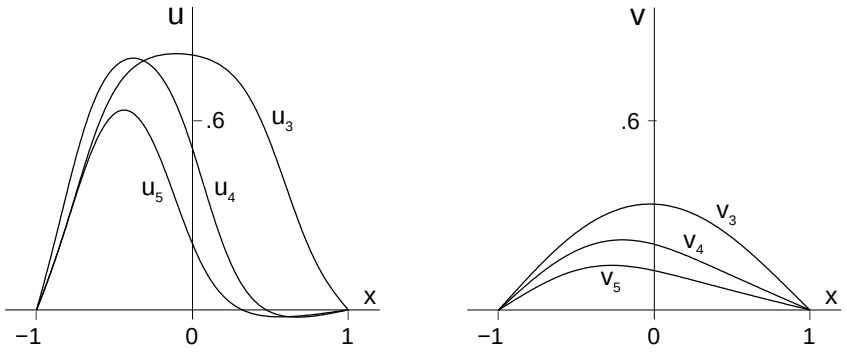

Figure 6: *Asymmetric solutions* u_3, u_4, u_5 *(left) and* v_3, v_4, v_5 *(right) of (7) on* A_1 *in Figure 4. The parameters are* $\varepsilon = .1$, *and* $\delta = .2$

symmetric solutions on S_1 and S_2. In Figure 6 we keep $\varepsilon = .1$ and $\delta = .2$ and show three asymmetric solutions on A_1.

4.1.4 ε in $[.08, .1)$

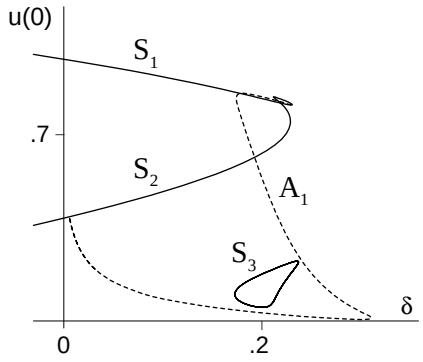

Figure 7: *Bifurcation curves of symmetric and asymmetric solutions:* $\varepsilon = .08$

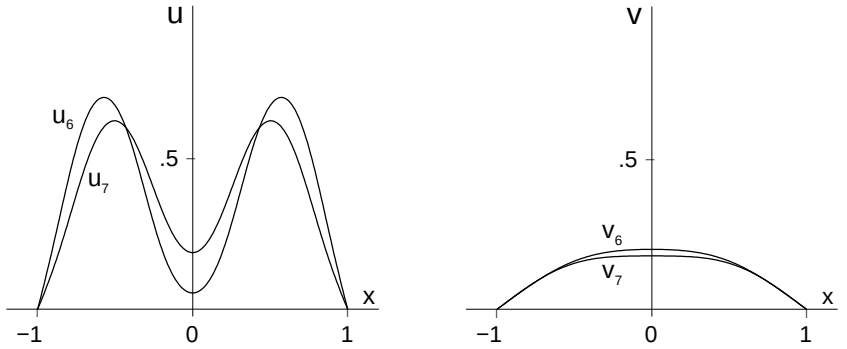

Figure 8: *Symmetric solutions* u_6, u_7 *(left) and* v_6, v_7 *(right) on* S_3 . *The parameters are* $\varepsilon = .08$, *and* $\delta = 0.2$

As ε decreases from $\varepsilon = .1$, we find a third critical value, $\varepsilon_3 \approx .817$, at which a new branch S_3 of symmetric solutions suddenly appears. In Figure 7 we compute this branch for $\varepsilon = .08$,

and see that it has the form of an 'island'. In Figure 8 we set $\varepsilon = .08$ and $\delta = .2$, and show the two positive, symmetric solutions on S_3.

4.1.5 $.08 > \varepsilon \geq .07$

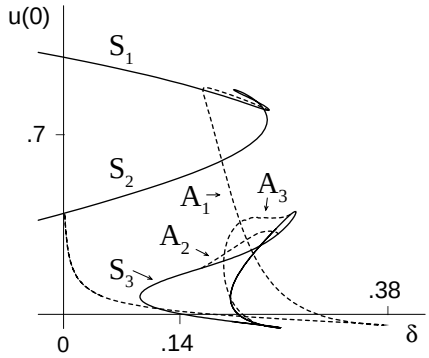

Figure 9: *Bifurcation diagram:* $\varepsilon = .07$

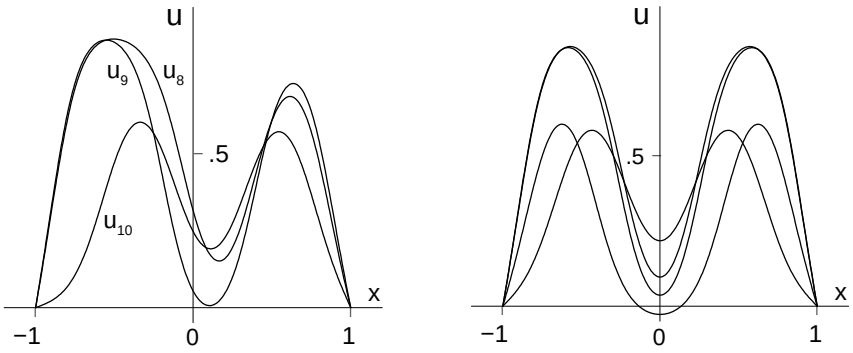

Figure 10: *Asymmetric solutions on* A_3 *and* A_2 *(left), and symmetric solutions on* S_3 *(right) for* $\varepsilon = .07$, $\delta = .2$ *in Figure 9.* u_8 *and* u_9 *are on* A_3 *and* u_{10} *is on* A_2.

In Figure 9 we set $\varepsilon = .07$ and see that the shape of S_3 has undergone a significant deformation into a more complicated structure. Now there are *two* new branches A_2 and A_3 of asymmetric solutions (dashed curves) which bifurcate from points on S_3. In Figure 10 we set $\varepsilon = .07$ and $\delta = .2$, and show seven symmetric and asymmetric solutions on S_3, A_2 and A_3.

4.1.6 ε **in** $[.05, .07)$

In Figure 11 we set $\varepsilon = .05$ and find that the bifurcation diagram becomes even more complicated. The three curves S_1, S_2 and S_3 representing families of symmetric solutions have now combined into one continuous curve in the $(\delta, u(0))$ plane. S_1 still denotes the stable solutions up to the first knee; S_2 denotes the saddles starting from the single peak for $\delta = 0$ up to first knee; the remainder is called S_3. In addition, the dashed curves A_2 and A_3, which denote families of asymmetric solutions in Figure 9, have also merged into one continuous curve. The branch A_1 continues to exist as well. Because problem (20) becomes singular as ε decreases, the behavior of the bifurcation curves in the neighborhood of $(\delta, u(0)) = (0, 0)$ is

unclear in left of Figure 11. Thus, to understand the diagram near $(\delta, u(0)) = (0, 0)$, we have blown up this region. Figure 12 adds the graphs of some corresponding u.

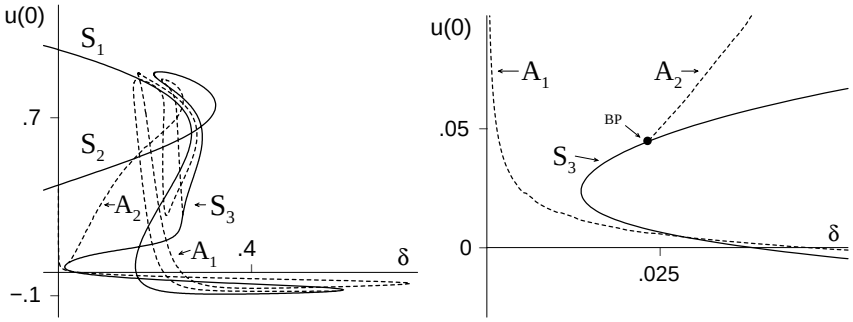

Figure 11: *Bifurcation diagram: $\varepsilon = .05$, with blow-up near 0.*

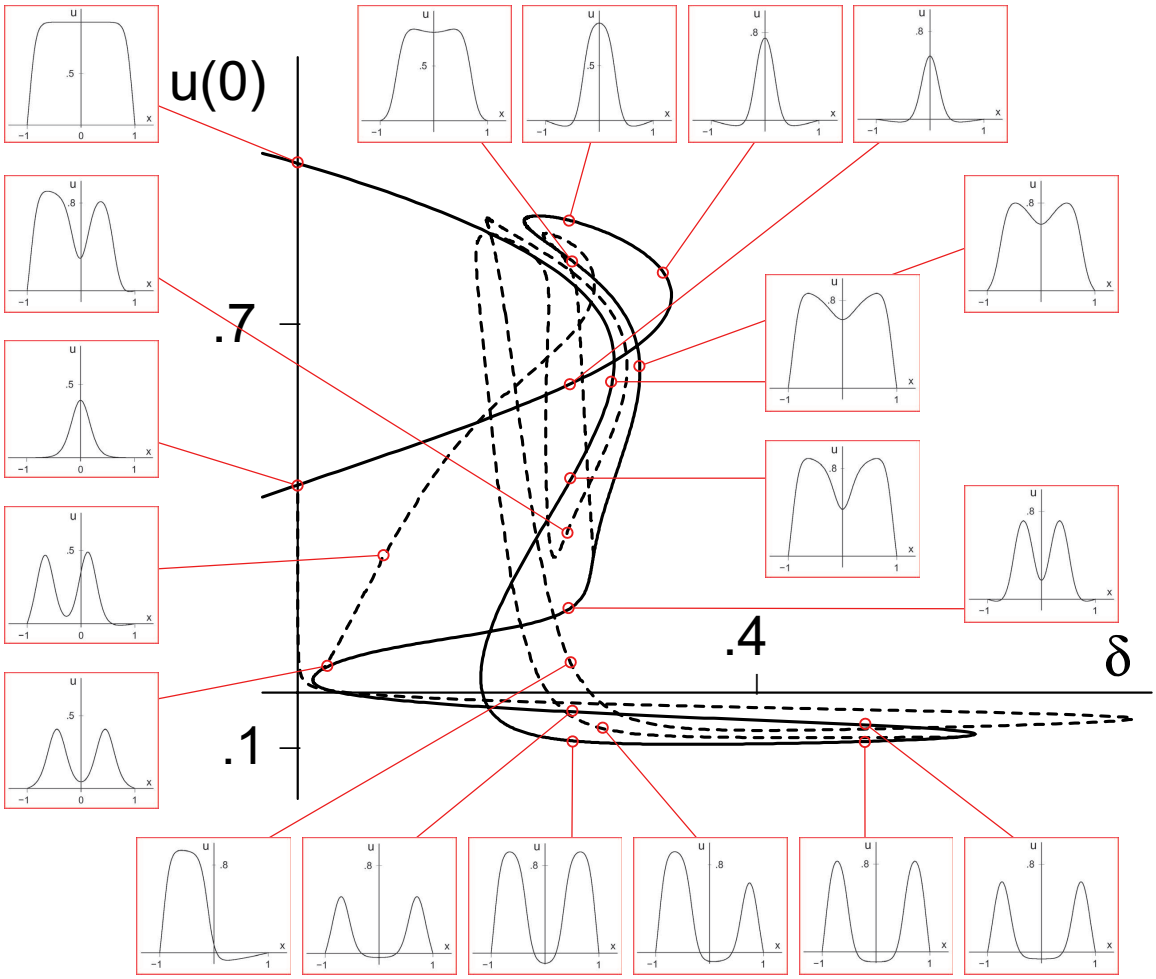

Figure 12: *Again Figure 11, now with some corresponding u: $\varepsilon = .05$*

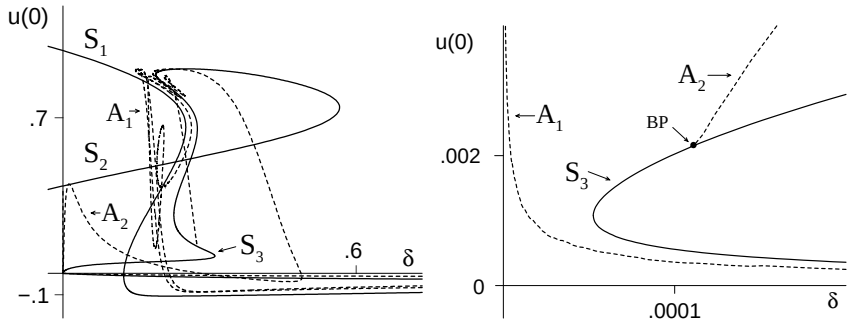

Figure 13: *Bifurcation diagram:* $\varepsilon = .03$

4.1.7 ε in $[.03, .05)$

Finally, we decrease ε to $\varepsilon = .03$ and see in Figure 13 that the bifurcation diagram has continued to deform into a more complicated structure still, with increasing numbers of folds in the curves representing both asymmetric and symmetric solutions. Again, on the right in Figure 13 we blow up the region near $(\delta, u(0)) = (0, 0)$ and find that structure of the bifurcation diagram is similar to that for the case $\varepsilon = .05$.

4.2 In two dimensions

Except when restricting oneself to the radially symmetric case one cannot proceed by a shooting or a similar argument in higher space dimensions. Hence we will have to use a different approach as for the one-dimensional case. We will consider the variational setting as in [24] and we will look for stationary functions of the energy functional $\Phi_\varepsilon : W_0^{1,2}(\Omega) \to \mathbb{R}$ defined by

$$\Phi_\varepsilon(u) = \frac{\varepsilon^2}{2} \int_\Omega |\nabla u|^2 \, dx + \frac{\delta}{2} \int_\Omega u \, \mathcal{G}(u) \, dx - \int_\Omega F(u) \, dx, \tag{22}$$

where $F(u) = \int_0^u f(s)ds = -\left(\frac{1}{4}u^2 - \frac{1}{3}(1+a)\,u + \frac{1}{2}a\right) u^2$ and $\mathcal{G}$ the Dirichlet Green operator, that is, $\mathcal{G}w$ is the solution of $-\Delta u = w$ in Ω with $u = 0$ on $\partial\Omega$. Indeed, due to the symmetry of the corresponding Green's function G a stationary function of Φ satisfies

$$\varepsilon^2 \int_\Omega \nabla u(x) \cdot \nabla \varphi(x) \, dx \; + \; \delta \int_\Omega \int_\Omega u(y) G(x,y) \varphi(x) \, dy \, dx \;\; = \;\; \int_\Omega f(u(x)) \, \varphi(x) \, dx \quad \text{for all } \varphi \in W_0^{1,2}(\Omega),$$

which means that u is a weak solution of

$$\begin{cases} -\varepsilon^2 \Delta u &= f(u) - \delta \mathcal{G}(u) & \text{in } \Omega, \\ u &= 0 & \text{on } \partial\Omega, \end{cases} \tag{23}$$

and hence of (3). Note that Φ_ε is coercive (see [24]) for $\delta \geq 0$:

1. $\Phi_\varepsilon(u) \to \infty$ when $\|u\|_{W^{1,2}(\Omega)} \to \infty$; we even have $\Phi_\varepsilon(u) \geq \frac{\varepsilon^2}{2} \|u\|^2_{W^{1,2}(\Omega)} - 1$ for $u \in W_0^{1,2}(\Omega)$;
2. $\Phi_\varepsilon(u) \leq \liminf_{m\to\infty} \Phi_\varepsilon(u_m)$ for $u, u_m \in W_0^{1,2}(\Omega)$ with $u_m \rightharpoonup u$.

Hence for every $\delta \geq 0$ the functional Φ_ε attains its minimum. In fact, for $\delta \geq 0$ but small there are multiple minima. Let us discuss these in more detail.

a. Since

$$\begin{aligned} -\int_\Omega F(u)\,dx &= \int_\Omega \left(\tfrac{1}{4}u^2 - \tfrac{1}{3}(1+a)\,u + \tfrac{1}{2}a\right)u^2 dx \\ &\geq \left(\tfrac{1}{2}a - \tfrac{1}{3}(1+a)\,|\Omega|^{-\frac{1}{3}}\,\|u\|_{L^2(\Omega)}\right)\|u\|^2_{L^2(\Omega)} \end{aligned}$$

the trivial solution $u = 0$ is a local minimum and $\Phi_\varepsilon(0) = 0$.

b. From [24] it is known that, if ε is sufficiently small, a bifurcation curve $\delta \mapsto u(\delta)$ starts from a boundary layer solution for the case $\delta = 0$. For δ small the solutions u_{bl} on this curve are local minimizers for the functional Φ_ε with $\Phi_\varepsilon(u_{bl}) < 0$. Such solutions can be approximated by a standard numerical minimization procedure.

c. In [24] it is also expected that there are $\delta_2 > \delta_1 > 0$ such that in the interval (δ_1, δ_2) the previous solutions are not global minimizers. Instead a solution with lower energy appears. Numerical evidence suggest that there are (global ?) minimizers which have both an boundary layer as well as an internal layer. It is shown that such a function u_{dl} satisfies $\Phi_\varepsilon(u_{dl}) < \Phi_\varepsilon(u_{bl})$. Also these can be numerically approximated by a minimization process that starts with an appropriate initial function.

4.2.1 Minimizers

Numerical tools for finding minimizers of an energy function, which are generically stable in the sense that the eigenvalues of the linearised problem have negative real part, are numerous. We have used an iteration scheme based on

$$u = \left(-\varepsilon^2\Delta + 1\right)^{-1}\left(f(u) + u - \delta\mathcal{G}u\right). \tag{24}$$

4.2.2 Mountain Pass

Different from [24] is that we have used a variation of the approach of Choi and McKenna, [2], to obtain mountain pass solutions. One should start with two functions that are guaranteed to lie on both sides of, and in energy below, a mountain pass. Candidates to start with are, for $\delta \in (\delta_1, \delta_2)$ any pair of the three local minimizers mentioned above, that is, the boundary layer solution u_{bl}, the double layer solution u_{dl} and the trivial solution 0. Before explaining the numerical procedure let us first define a polygon:

$$\begin{aligned} [u_1, u_2] &:= \{u_1 + t\,(u_2 - u_1)\,; 0 \leq t \leq 1\}, \\ [u_1, u_2, u_3, \ldots, u_m] &:= [u_1, u_2] \cup [u_2, u_3] \cup \cdots \cup [u_{m-1}, u_m]. \end{aligned}$$

We call $\{u_1, u_2, u_3, \ldots, u_m\}$ the vertices of the polygon $[u_1, u_2, u_3, \ldots, u_m]$. The procedure we used initially is roughly described as follows. Find the maximum on the curve and bend the curve away at this point in direction opposite to the gradient of the functional. See Figure 14 and 15.

4.2.3 Tango, a numerical inner variation

It turned out that the straightforward implementation of the Mountain Pass Algorithm failed to give convergence of the maximizer of the polygon to the solution we expected. Indeed, these maximizers did converge to a function that locally resembles a peak-shaped solution

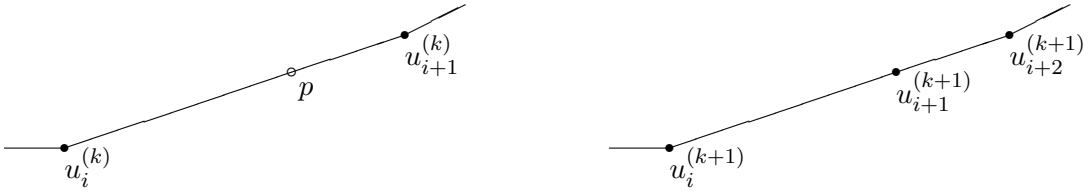

Figure 14: *If the energy function has an interior maximum on the line* $[u_i^{(k)}, u_{i+1}^{(k)}]$ *one inserts this* p *in the polygon.*

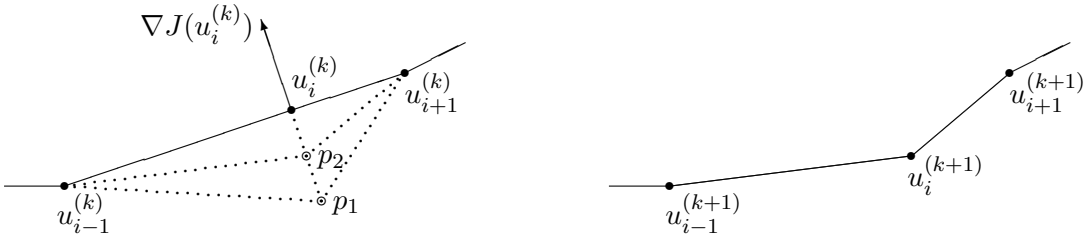

Figure 15: *If the energy function has an maximum in* $u_i^{(k)}$*, the gradient* $\nabla J(u_i^{(k)})$ *is computed and one tests the maximal energy on a curve that is moved in the opposite direction. If the new curve* $[u_{i-1}, p_1, u_{i+1}]$ *does not lower the maximal energy one moves half as far (*$\frac{1}{4}$ *as far, etc.).*

but the location of the peak was not where expected. In fact, some experiments showed that by modifying the initial curve we could obtain a peak at any location. As is well known for the location of the peak-solution for the single equation (see [21] or [5]) the location of the peak and the shape of the peak are governed by procedures of different order. Our impression is that a grid-locking phenomenon (the numerical approximation tends to fit to grid-points in an optimal configuration) prevents the approximation to move to the expected analytically optimal location. To overcome this phenomenon we introduced an inner variation step as follows. In each iteration we checked if the function of maximal energy on the curve shifted moved one grid-step in the north, east, south, respectively west direction did have a lower energy. If it did we modified the polygon by replacing the vertex by the shifted function.

4.2.4 Summary of the procedure

Algorithm 6 *(1) Choose two initial functions* u_{begin}, u_{end} *that lie on two sides of a mountain range. Compute the maximum* u_M *of* Φ_ε *on* $\Gamma_0 = [u_{begin}, u_{end}]$ *and set*

$$\Gamma := [u_{begin}, u_M, u_{end}]\,.$$

(2) Compute the maximum u_M *of* Φ_ε *on the vertices of* Γ *and set* $\phi = \nabla\Phi_\varepsilon(u_M)$*.*

(a) Set $u_* = u_M - \phi$ *and compute* $u_{*1} \in [u_{M-1}, u_*]$*, respectively* $u_{*2} \in [u_*, u_{M-1}]$*, such that*

$$\begin{aligned}\Phi_\varepsilon(u_{*1}) &= \max\{\Phi_\varepsilon(u)\,;u \in [u_{M-1}, u_*]\}\,,\\ \Phi_\varepsilon(u_{*2}) &= \max\{\Phi_\varepsilon(u)\,;u \in [u_*, u_{M+1}]\}\,.\end{aligned}$$

(b) If $\max\{\Phi_\varepsilon(u_{*1}), \Phi_\varepsilon(u_{*2})\} > \Phi_\varepsilon(u_M)$*, then* $\phi := \frac{1}{2}\phi$ *and return to (a).*

(c) Replace u_M *by* u_* *in* Γ :

$$\Gamma := [u_{begin}, \ldots, u_{M-1}, u_*, u_{M+1}, \ldots . u_{end}] .$$

If $u_{*1} \notin \{u_{M-1}, u_*\}$, *then add* u_{*1} :

$$\Gamma := [u_{begin}, \ldots, u_{M-1}, u_{*1}, u_*, u_{M+1}, \ldots . u_{end}] .$$

If $u_{*2} \notin \{u_*, u_{M+1}\}$, *then add* u_{*2} :

$$\Gamma := [u_{begin}, \ldots, u_*, u_{*2}, u_{M+1}, \ldots . u_{end}] .$$

(3) Compute the maximum u_M *of* Φ_ε *on the vertices of* Γ. *Compute the energy of the shifted functions* $u_M(\cdot - s)$, *with* s *a one grid-step shift. If the energy is lower then replace* u_M *by* $u_M(\cdot - s)$ *and if necessary introduce as in step (2.c) additional vertices and repeat (3). To prevent loops we put a bound to the number of repetitions for this cycle.*

(4) Consider the vertex u *of* Γ *where* $(\Phi_\varepsilon)_\Gamma$ *has its maximum. If its gradient is sufficiently small, then this vertex* u *approximates the mountain pass solution and one stops. Otherwise return to (2).*

Let us remark that $\psi = \nabla \Phi_\varepsilon (u)$ is such that

$$\begin{aligned} \int_\Omega \psi (x) \varphi(x) \quad &= \quad \varepsilon^2 \int_\Omega \nabla u(x) \cdot \nabla \varphi(x) \, dx \; + \; \delta \int_\Omega \int_\Omega u(y) G(x,y) \varphi(x) \, dy \, dx \\ &\quad - \int_\Omega f (u(x)) \varphi(x) \, dx \text{ for all } \varphi \in W_0^{1,2}(\Omega). \end{aligned}$$

Hence $\psi = -\varepsilon^2 \Delta u - f(u) + \delta \mathcal{G} u$ which is defined in $W^{-1,2}(\Omega)$ for $u \in W_0^{1,2}(\Omega)$.

4.2.5 Outcome

For our numerical experiments we have chosen a simple nonradial domain, namely the square $\Omega = (0,1) \times (0,1)$. We have fixed $\varepsilon = 0.03$ and considered $\delta \in \{0, .05, .2, .35, .8\}$.

For the stable solutions we copied the approach in [24] and started with the boundary layer solution $u_{bl,0}$ for $\delta = 0$ as well as with an artificial double layer function $u_{dl,0}$. Another initial function that we started with is a boundary layer solution $u^0_{blsub,0}$ on a small subdomain near the center, or with $u^i_{blsub,0}$ for $i = 1, 2, 3$ on a small subdomain moved away from the center, respectively in north-west, north-north-west and north direction. Let us denote $\Gamma^1_\delta = [u_{bl,\delta}, u_{dl,\delta}]$, $\Gamma^2_\delta = [0, u_{bl,\delta}]$, $\Gamma^3_\delta = [0, u_{dl,\delta}]$ and $\Gamma^{0,i} = [0, u^i_{blsub,0}]$. In Table 1 one finds a listing of the starting points and the approximated solution we obtained.

The computations for the stable solutions and for a first mountain pass solution, u_{dip}, did not use the symmetry of the square. Nevertheless all numerical approximations that came out did have the maximal symmetry for the square. For the mountain pass solutions with one of more peaks the fine grid made it necessary for the size of the computations to exploit the full symmetry. Only the one-corner-peak has been computed without using any symmetry but on a less fine grid. In all other cases we computed a solution of the corresponding problem on the triangle (1/8-th square). With some imagination a curve like $S_1 - S_2 - S_3$ in Figure 11 fits through. See Figure 16. In Figure 20 and 21 we show some of the peak-functions that we expect to approximate solutions.

grid	δ :	0	.05	.20	.35	.80
40×40	boundary layer	1 $u_{bl,0}$	$u_{bl,0}$ $u_{bl,.05}$	$u_{bl,0}$ $u_{bl,.2}$	$u_{bl,0}$ $u_{bl,.35}$	—
40×40	double layer	—	—	—	$u_{dl,0}$ $u_{dl,.35}$	$u_{bl,0}$ $u_{dl,.8}$ $u_{dl,0}$ $u_{dl,.8}$
$\frac{1}{8}^{th}$ of 80×80	boundary + dip	—	—	—	$\Gamma^1_{.35}$ $u_{dp,.35}$	—
40×40	one corner peak*)	—	—	—	$\Gamma^{0,1}$ $u_{cp,.35}$ $\Gamma^{0,2}$ $u_{cp,.35}$	—
$\frac{1}{8}^{th}$ of 80×80	center peak	$\Gamma^{0,0}$ $u_{pk,0}$ $\Gamma^{0,1}$ $u_{pk,0}$	$\Gamma^{0,0}$ $u_{pk,.05}$	$\Gamma^{0,0}$ $u_{pk,.2}$	$\Gamma^{0,0}$ $u_{pk,.35}$	—
$\frac{1}{8}^{th}$ of 80×80	four corner peaks	—	$\Gamma^2_{.05}$ $u_{fpc,.05}$	$\Gamma^2_{.2}$ $u_{fpc,.2}$	$\Gamma^2_{.35}$ $u_{fpc,.35}$ $\Gamma^3_{.35}$ $u_{fpc,.35}$ $\Gamma^{0,1}$ $u_{fpc,.35}$ $\Gamma^{0,2}$ $u_{fpc,.35}$	$\Gamma^3_{.8}$ $u_{fpc,.8}$
$\frac{1}{8}^{th}$ of 80×80	four side peaks	—	—	—	$\Gamma^{0,3}$ $u_{fps,.35}$	—

Table 1: *List of the numerical results on the square:* $\varepsilon = .03$. *The boundary layer and double layer solutions have been obtained by an iteration scheme for stable solutions. These two and the trivial solution were the only ones that resulted from that iteration scheme (see Section 4.2.1). All other solutions are obtained by the mountain pass algorithm and hence generically are unstable. By* $\frac{1}{8}^{th}$ *of* 80×80 *we mean that using symmetry assumptions the actual computation took place on a triangular grid with a side of* 40 *points. For* $\delta = .35$ *we started, next to the two initial curves mentioned, with a curve connecting* 0 *with a rather wild function of negative energy. Since even that process eventually converged to a peak at a corner (here the north-east corner) the algorithm appears quite stable with respect to initial functions.*

5 Conclusions

In this paper we have incorporated a combination of analytical and numerical techniques to obtain new insights into the mechanisms responsible for pattern formation in the FitzHugh-Nagumo equations. The parameter regime we study is complementary to that of earlier studies of activator-inhibitor models. Beginning with the one-dimensional problem (3), our numerical results reveal how the structure of bifurcation curves in the (u, δ) plane highlight the complicated connections that exist between families of symmetric and asymmetric solutions. Using the one-dimensional results as a guide, we have also investigated pattern formation in the full two-dimensional partial differential equation system (2). Here we have developed new algorithms to find both stable (i.e. local mimimizers) and unstable symmetric solutions, several of which were previously unreported. In addition, we have found a surprising new type of asymmetric solution (Figure 17, right panel).

Our results suggest a number of natural extensions. Amongst the important issues for future research are the following:

1. Depending on the range of δ, system (2) produces at least four stable solution(s), respecively 0, u_{bl}, u_{dl} (Figures 17 and 18), and the new 'chimney' shaped solution shown

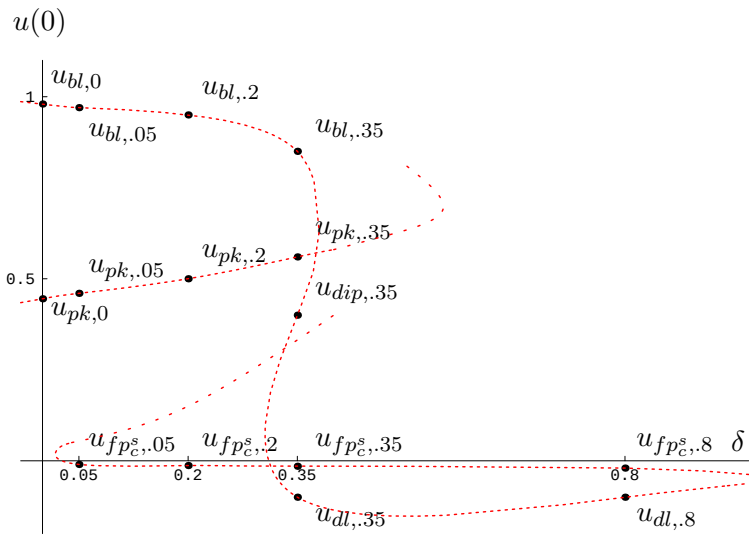

Figure 16: *Impression for part of a bifurcation diagram on a square:* $\varepsilon = .03$

in Figure 22. In addition, several new unstable solutions were found (Figures 19–21). Although rigorous existence proofs are still missing, the present numerical results are quite convincing. For $\gamma \neq 0$, but close to 0, it seems that the situation we have found will hardly change. Could it be different for bigger γ?

2. Dancer and Yan showed in [6] that for $\varepsilon \downarrow 0$ the global minimizer is of type u_{bl} for $\delta \leq \delta_0$ and of boundary layer with 'wild' internal behaviour if $\delta > \delta_0$. 'Wild' meaning that except for a uniform neighborhood of the boundary (that is, not depending on ε) the minimizing solution 'jumps' between the smallest and largest zero of $f(u) - \tau$ with τ defined by an equal area condition. For our $a = \frac{1}{4}$ it means u jumping between two zeroes of $f(u) - f(\frac{5}{12})$, namely -0.10375 and 0.937083. The first 'jumping' solution that we could obtain numerically is depicted in Figure 22. Enlarging ε (or reducing δ) the interior tube shrinks to a peak and almost immediately collapses to the double-layer solution we denoted by u_{dl}. Reducing ε we expect the tube to widen. Eventually a solution will appear having a boundary layer and a wide tube but also a new peak in the center. Next this peak will turn into a tube and move outwards. However, due to the small size of ε we have not been able to verify this numerically. For fixed $\delta > \delta_0$ [6] proves that the minimizer is of 'wild' type, which in the present convex domain would probably mean a series of concentric tubes. Nevertheless, we still expect that there is $\delta_\varepsilon > \delta_0$ such that for $\delta = \delta_\varepsilon$ the global minimizer is of u_{dl}-type. Any rigorous results in this direction would be very interesting.

3. The numerical nature of the present saddle point solutions is very sensitive. It made it very hard to find the correct balance between lowering the mountain crossing by 'outer variation', i.e. moving by the gradient, and by 'inner variation', the one step shift. Appropriate algorithms, with or without our 'tango' sub-algorithm, are still open for improvement.

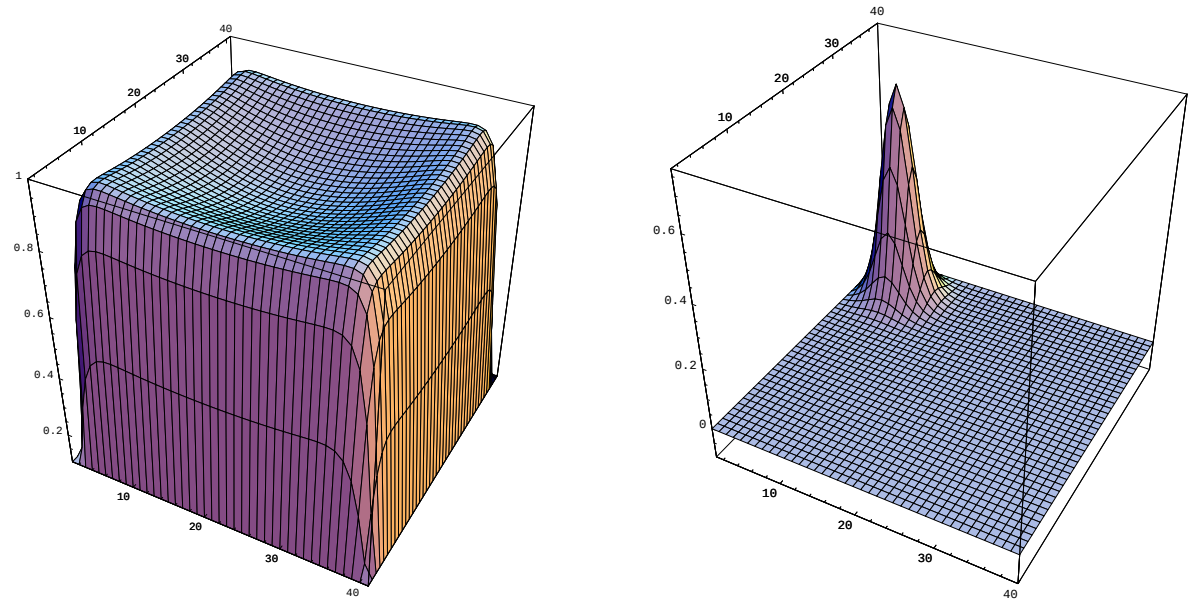

Figure 17: *The stable boundary layer solution,* $u_{bl,.35}$ *and the 'lowest' mountain pass* $u_{cp,.35}$*;* $\varepsilon = .03$ *and* $\delta = .35$.

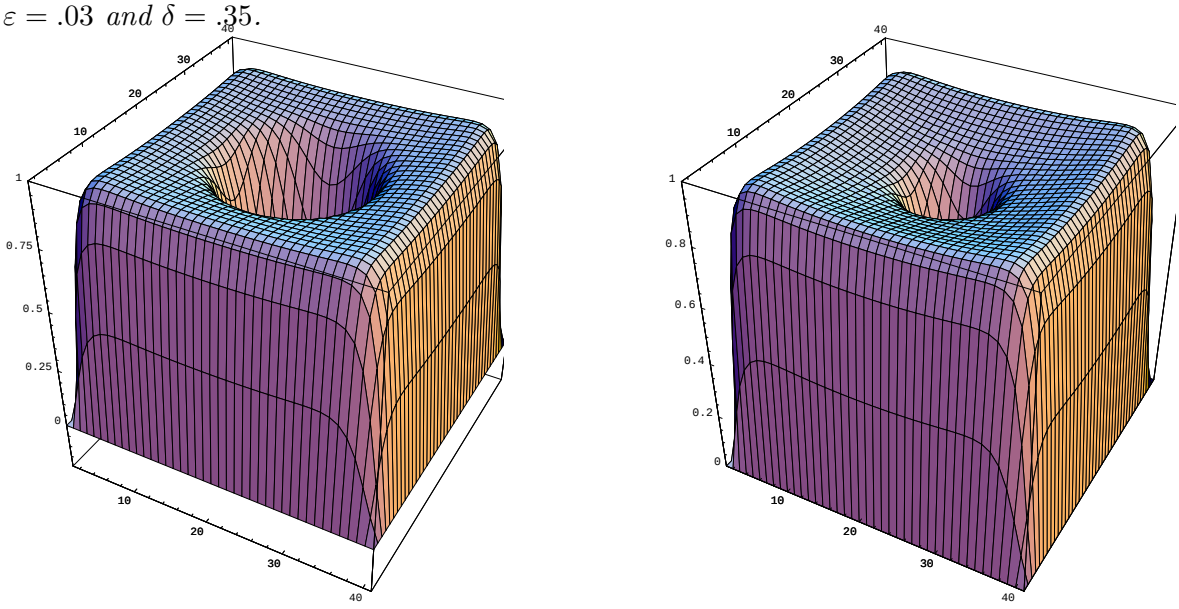

Figure 18: *A stable double layer solution,* $u_{dl,35}$*, and a mountain pass,* $u_{dip,.35}$*:* $\varepsilon = .03$ *and* $\delta = .35$.

References

[1] Aliev, R.R.; Panilov, A.V. A simple two-variable model of cardiac excitation. *Chaos, Solitons and Fractals* 7 (1996), 293–301.

[2] Choi, Y. S.; McKenna, P. J. A mountain pass method for the numerical solution of semilinear elliptic problems. *Nonlinear Anal.* 20 (1993), no. 4, 417–437.

[3] Clément, Ph.; Sweers, G. Existence and multiplicity results for a semilinear elliptic eigenvalue problem. *Ann. Scuola Norm. Sup. Pisa Cl. Sci.* (4) 14 (1987), no. 1, 97–121.

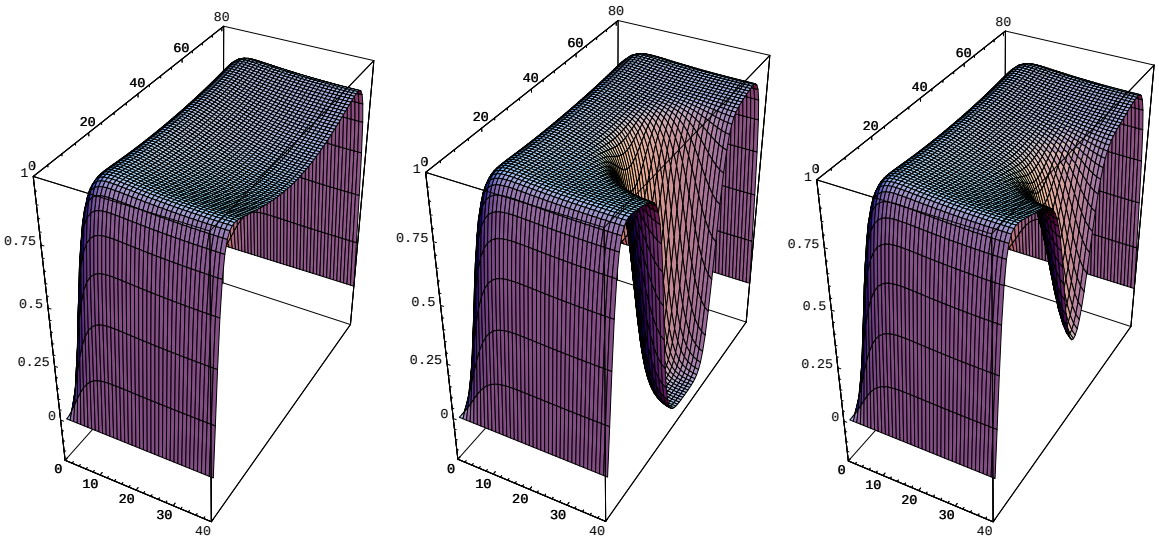

Figure 19: *Cut-open versions of the previous 3 solutions with a boundary layer on a finer grid: resp.* $u_{bl,.35}$, $u_{dl,.35}$ *and* $u_{cp,.35}$. *The first two are obtained by the iteration process for stable solutions; the third one by the mountain-pass algorithm.*

[4] Crandall, M.G.; Rabinowitz, P.H. Bifurcation from simple eigenvalues. *J. Functional Anal.* 8 (1971), 321-340.

[5] Dancer, E. N.; Wei, Juncheng On the location of spikes of solutions with two sharp layers for a singularly perturbed semilinear Dirichlet problem. *J. Differential Equations* 157 (1999), no. 1, 82–101.

[6] Dancer, E. N.; Shusen Yan, A minimization problem associated with elliptic systems of FitzHugh-Nagumo type, preprint.

[7] Doedel, E.; Champneys, A. R.; Fairgrieve, T. F.; Kutznetsov, Y. A.; Standstede, B.; Wang, X. AUTO97: Continuation and bifurcation software for ordinary differential equations, 1997.

[8] Ermentrout, G.B.; XPPAUT, Version 5.0. available at `www.math.pitt.edu/~phase/`

[9] Ermentrout, G.B.; Hastings, S.P.; Troy, W.C. Large amplitude stationary waves in an excitable lateral-inhibitory medium. *SIAM J. Appl. Math.* 44 (1984), no. 6, 1133–1149.

[10] De Figueiredo D.G.; Mitidieri E. A maximum principle for an elliptic system and applications to semilinear problems. *SIAM J. Math. Anal.*, 17 (1986), 836–849.

[11] FitzHugh, R. Impulses and physiological states in theoretical models of nerve membrane. *Biophys. J.* (1961), no. 1-2, 445–466.

[12] Garcia-Melián, J.; Sabina de Lis, J. Stationary patterns to diffusion problems, *Math. Meth. Appl. Sci.*, 23 (2000), 1467-1489.

[13] Gardner, R.; Peletier, L.A. The set of positive solutions of semilinear equations in large balls. *Proc. Roy. Soc. Edinburgh Sect. A* 104 (1986), no. 1-2, 53–72.

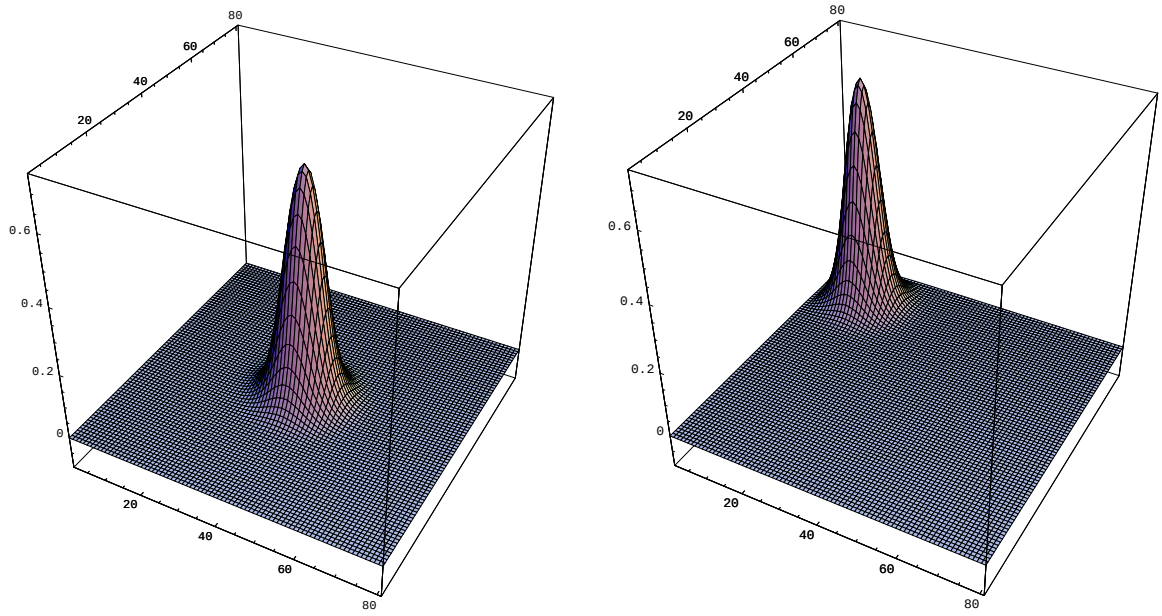

Figure 20: *A mountain pass solution under symmetry, $u_{pk,.35}$ and for comparison, again the 'lowest' (non-symmetrical) mountain pass solution having the peak in the corner $u_{cp,.35}$. : $\varepsilon = .03$ and $\delta = .35$.*

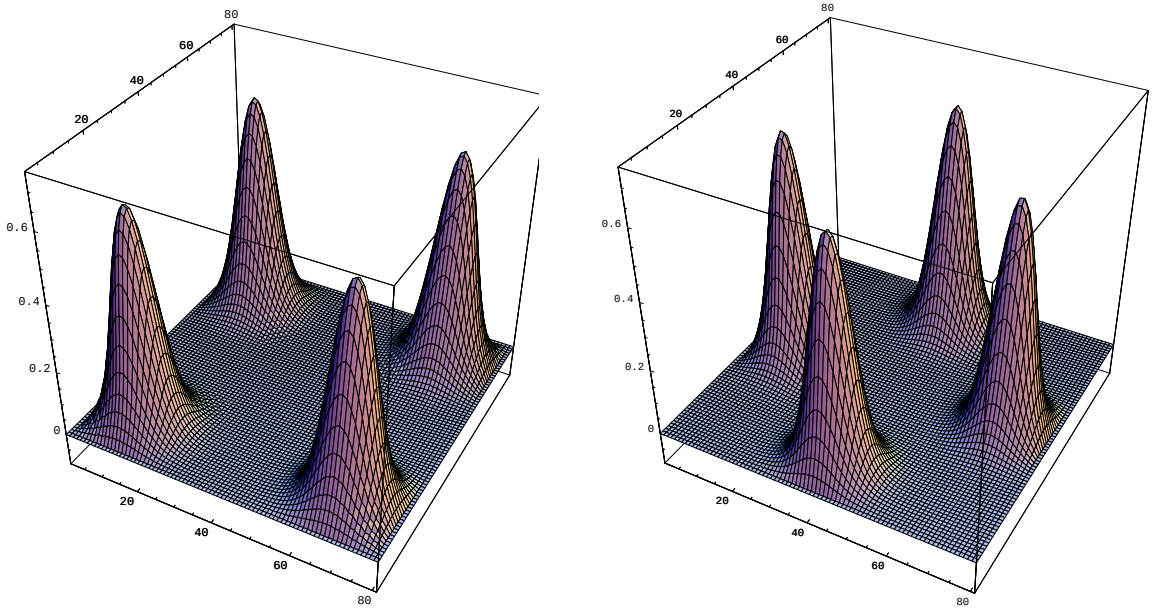

Figure 21: *Two mountain pass solutions, peaking in the corners, $u_{fpc,.35}$, resp. peaking at the sides, $u_{fps,.35}$: $\varepsilon = .03$ and $\delta = .35$.*

[14] Hodgkin, A.; Huxley, A. A quantitative description of membrane current and its application to conduction and excitation in nerve. *Jour. Physiol.,* London, 117 (1952), 500–544.

[15] Hargerg, A.; Meron, E. From labyrinth patterns to spiral turbulence. *Phys. Rev.. Lett.* 72 (1994), 2494–2497.

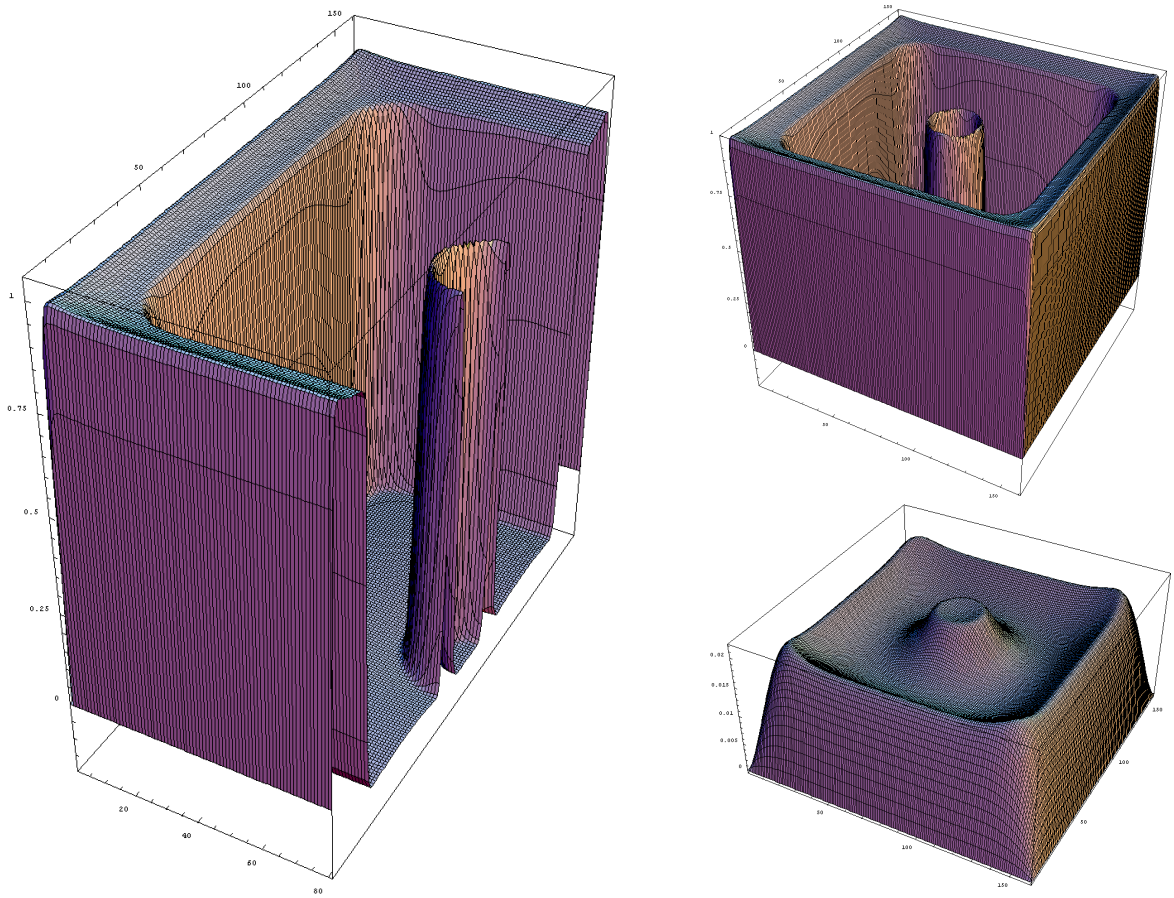

Figure 22: *For ε much smaller than previously considered, a new stable solution appears with a more complicated structure. Solution with multiple jumps in the interior are predicted in [6]. Depicted are resp. u cut-open and full, and the corresponding v: $\varepsilon = .005$ and $\delta = 2$. We have not been able to find a numerical confirmation of a solution with such behaviour for $\varepsilon \geq .01$.*

[16] Goldstein, R. E.; Muraki, D. J.; Petrich, D. M. Interface proliferation and the growth of labyrinths in a reaction-diffusion system. *Phys. Rev. E* 53 (1996), 3933–3957.

[17] Klaasen, G.A.; Troy, W.C. Stationary wave solutions of a system of reaction-diffusion equations derived from the FitzHugh-Nagumo equations. *SIAM J. Appl. Math.* 44 (1984), 96–110.

[18] Klaasen, G.A.; Mitidieri, E. Standing wave solutions for a system derived from the FitzHugh-Nagumo equations for nerve conduction. *SIAM J. Math. Anal.*, 17 (1986), 74–83.

[19] Mimura, M.; Nishiura, Y. Layer oscillations in reaction-diffusion systems. *SIAM J. Appl. Math.* 49 (1989), 481–514.

[20] Nagumo, J.S.; Arimoto, S. ; Yoshizawa, Y. An active pulse transmission line simulating nerve axon. *Proc. Inst. Radio. Engineers* 50 (1962), 2061–2070.

[21] Ni, Wei-Ming; Takagi, Izumi; Wei, Juncheng. On the location and profile of spike-layer solutions to a singularly perturbed semilinear Dirichlet problem: intermediate solutions. *Duke Math. J.* 94 (1998), no. 3, 597–618.

[22] Nishiura, Y.; Mimura, M.; Ikeda, H.; Fujii, H. Singular limit analysis of stability of traveling wave solutions in bistable reaction-diffusion systems. *SIAM J. Math. Anal.* 21 (1990), no. 1, 85–122.

[23] Rabinowitz, P.H. Some global results for nonlinear eigenvalue problems. *J. Functional Analysis* 7 (1971), 487–513.

[24] Reinecke, C.J.; Sweers, G. Solutions with internal jump for an autonomous elliptic system of FitzHugh-Nagumo type.

[25] Rogers, J.M.; McCullough, A.D. A collocation-Galerkin finite element model of cardiac action potential propagation. *IEEE Trans. Biomed. Eng.* 3 (1994), no. 41, 743–757.

[26] Smoller, J.; Wasserman, A. On the monotonicity of the time-map. *J. Differential Equations* 77 (1989), no. 2, 287–303.